Fixational Eye Movement Radar: Random Spatial Modulation

Garrett Zook, Patrick McCormick, Shannon D. Blunt
Radar Systems Lab (RSL), University of Kansas, Lawrence, KS

***Abstract*—It was recently shown that it is possible to mimic the passive actuation of the human eye, otherwise known as fixational eye movement (FEM), using an active MIMO FM radar emission and associated receive processing. Given that biological FEM possesses an inherent randomness, here the use of FM noise radar waveforms and random spatial jittering are incorporated into this active emission structure to realize FEM radar (FEMR). Note that in contrast to standard beam dithering or MIMO radar, FEMR forms a completely coherent beam that varies spatially with time. It is shown that FEMR intrinsically enhances spatial resolution in both azimuth and elevation relative to standard (fixed) beamforming using only matched filter processing.**

Keywords—biomimetic sensing, MIMO radar, waveform diversity

I. Introduction

Echo-locating mammals (e.g. bats, dolphins, and whales) use bio-sonar to navigate their environment and detect, localize, discriminate, pursue, and capture prey [1-10]. As such, despite what could be considered "mediocre equipment" [9] compared to sophisticated radar systems, these biological instantiations can still out-perform manmade systems in many respects, thus spurring a continued interest in biomimetic capabilities.

Here we specifically explore the potential that may be facilitated by using waveform diversity [11,12] to mimic the attributes of fixational eye movement (FEM) that occur in the human eye and other animals that possess fovea [13-15]. The operation of FEM involves a small, seemingly random modulation of the eye, denoted as microsaccades, around the actual direction of attention. The current consensus among biologists is that FEM improves visual acuity because the transients from this motion enhance contrast and sensitivity as well as aid in the resolution of spatial ambiguities. There is also evidence [15] that these eye movements adapt according to the amount of available lighting and the active attention of the observer, thereby suggesting a linkage between the physical actuation of the eye and aspects of cognition that may prove useful for cognitive radar [16].

It was recently shown [17-20] that a generalization of the polyphase-coded FM (PCFM) [21] structure to include coding for changes in spatial angle realizes an active emission that mimics FEM via a specific form of MIMO comprised of FM waveforms. Denoted as "spatial modulation", the original form involved fast-time sweeping of the coherent transmit beam generated by a phased array via determination of the spatial coding. This formulation subsumes the waveform-diverse class of signals known as the frequency-diverse array (e.g. see [22-25]) and, because it is dependent on an underlying coding that is completely arbitrary, has far greater freedom in how the beam sweeps in fast-time. Here this freedom is demonstrated through the incorporation of different forms of random spatial modulation combined with FM noise radar waveforms, with the ultimate goal of truly mimicking the nature of biological FEM for active radar emissions.

II. Spatially-Modulated FM Noise Radar

The fixational eye movement radar (FEMR) emission scheme involves the combination of the spatial modulation MIMO framework from [17-20] and FM noise waveforms [26-28]. The latter is realized via the pseudo-random optimized (PRO) FM approach that produces random FM waveforms designed to provide relatively low range sidelobes through the use of spectral shaping, which also has the side benefit of good spectral containment. Different random instantiations of spatial modulation are then used in conjunction with this random waveform to provide emissions that are randomly modulated in the azimuth and elevation dimensions as well.

A. PRO-FM Waveforms

The original PRO formulation [17] involved the design of a random frequency-modulated continuous-wave (FMCW) waveform in a piece-wise manner by optimizing each segment of duration T and then connecting it to the previous segment with an appropriate phase rotation to avoid discontinuities. We use this same format here so that it is possible to direct different segments of the waveform to different spatial look directions in addition to the random spatial modulation.

Each of the L segments is optimized to possess a power spectrum that closely approximates a desired power spectrum $|G(f)|^2$, thereby also specifying the autocorrelation of the segment. Here a Gaussian shape is chosen for $|G(f)|^2$ since the associated autocorrelation theoretically has no sidelobes.

Each segment is initialized with a random instantiation of a PCFM waveform [21] denoted as $s_{0,\ell}(t)$ for $\ell = 1,\ldots,L$. An alternating projections procedure is then applied iteratively to realize segments that closely approximate the desired power spectrum while also being constant amplitude. The kth iteration of this process for the ℓth segment performs the projection

$$r_{k+1,\ell}(t) = \mathbb{F}^{-1}\left\{ \left|G(f)\right| \exp\left(j\angle \mathbb{F}\left\{ s_{k,\ell}(t) \right\} \right) \right\} \tag{1}$$

This work was supported by the Office of Naval Research under Contract #N00014-16-C-2029. DISTRIBUTION STATEMENT A. Approved for Public Release.

where $\mathbb{F}\{\bullet\}$ is the Fourier transform, $\mathbb{F}^{-1}\{\bullet\}$ is the inverse Fourier transform, and $\angle(\bullet)$ extracts the phase of the argument. Since the amplitude of $r_{k+1,\ell}(t)$ likely does not meet the constant amplitude condition or duration limit of T, the second projection is performed as

$$s_{k+1,\ell}(t) = u(t)\exp\left(j\angle r_{k+1,\ell}(t)\right), \quad (2)$$

for $u(t)$ a rectangular window of length T. Alternating between (1) and (2) for K iterations allows the solution to descend onto a waveform that closely satisfies both requirements [29,30]. To avoid phase discontinuities the final ℓth optimized segment is phase rotated as

$$s_\ell(t) = \exp\left(j\phi_{\mathrm{end},\ell-1}\right) s_{K,\ell}(t), \quad (3)$$

where $\phi_{\mathrm{end},\ell-1}$ is the phase at the end of $(\ell-1)$th segment.

B. 2-D Spatial Modulation

Spatial modulation involves a particular form of MIMO in which a coherent beam is formed and then moved as a function of fast-time [17-20]. To permit beamsteering in both azimuth and elevation directions, consider the uniform planar array (UPA) in Fig. 1, which has M_{X} horizontal elements and M_{Z} vertical elements in the x-z plane with inter-element spacing d. The parameters ψ and θ represent the azimuth and elevation angles with respect to array boresight.

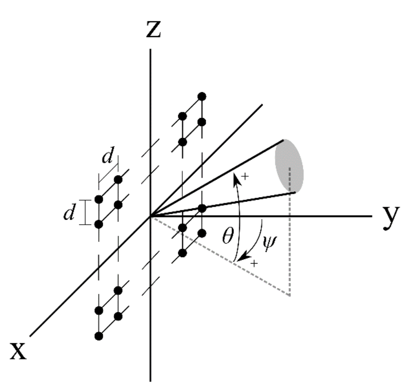

Fig. 1. Uniform planar array geometry

The array elements are indexed relative to the center of the array at coordinate location (0, 0) via

$$m_{\mathrm{X}} = \frac{-(M_{\mathrm{X}}-1)}{2}, \frac{-(M_{\mathrm{X}}-1)}{2}+1, \ldots, \frac{+(M_{\mathrm{X}}-1)}{2} \quad (4)$$

and

$$m_{\mathrm{Z}} = \frac{-(M_{\mathrm{Z}}-1)}{2}, \frac{-(M_{\mathrm{Z}}-1)}{2}+1, \ldots, \frac{+(M_{\mathrm{Z}}-1)}{2}. \quad (5)$$

Under the narrowband assumption the associated wave numbers are [31]

$$k_{\mathrm{X}}(\psi,\theta) = \frac{2\pi d}{\lambda}\sin\psi\cos\theta \quad (6)$$

and

$$k_{\mathrm{Z}}(\theta) = \frac{2\pi d}{\lambda}\sin\theta, \quad (7)$$

with wavelength λ corresponding to the center frequency.

Relative to center look direction $(\psi_{\mathrm{C}},\theta_{\mathrm{C}})$, the fast-time beam steering is specified using a length $N+1$ code of spatial offsets defined as $\{\Delta_0^{\mathrm{az}}, \Delta_1^{\mathrm{az}}, \ldots, \Delta_N^{\mathrm{az}}\}$ and $\{\Delta_0^{\mathrm{el}}, \Delta_1^{\mathrm{el}}, \ldots, \Delta_N^{\mathrm{el}}\}$ in azimuth and elevation, respectively. Thus, during the nth code interval the coherent beam sweeps from $(\psi_{n-1},\theta_{n-1})$ to the directions dictated by $\psi_n = \psi_{\mathrm{c}} + \Delta_n^{\mathrm{az}}$ and $\theta_n = \theta_{\mathrm{c}} + \Delta_n^{\mathrm{el}}$.

To realize continuous waveforms via PCFM, the electrical angle phase changes are defined as

$$\varepsilon_{\mathrm{x},n} = \frac{2\pi d}{\lambda}\left[\sin\psi_n\cos\theta_n - \sin\psi_{n-1}\cos\theta_{n-1}\right] \quad (8)$$

for azimuth and

$$\varepsilon_{\mathrm{z},n} = \frac{2\pi d}{\lambda}\left[\sin\theta_n - \sin\theta_{n-1}\right] \quad (9)$$

for elevation. The electrical phase-change sequences from (8) and (9) for $n = 1,\ldots,N-1$ are collected into the $N\times 1$ vectors $\mathbf{x}_{\mathrm{x}} = [\varepsilon_{\mathrm{x},1}, \ldots, \varepsilon_{\mathrm{x},N}]^T$ and $\mathbf{x}_{\mathrm{z}} = [\varepsilon_{\mathrm{z},1}, \ldots, \varepsilon_{\mathrm{z},N}]^T$ that parameterize the spatial modulation in azimuth and elevation.

Thus the 2D spatially modulating signals are [19,20]

$$b_{\mathrm{x}}(t;\mathbf{x}_{\mathrm{x}}) = \exp\left\{-j\left(\sum_{n=1}^{N}\varepsilon_{\mathrm{x},n}\int_0^t g(\zeta-(n-1)T_{\mathrm{p}})d\zeta + \bar{\Delta}_{\mathrm{x},0}\right)\right\} \quad (10)$$

and

$$b_{\mathrm{z}}(t;\mathbf{x}_{\mathrm{z}}) = \exp\left\{-j\left(\sum_{n=1}^{N}\varepsilon_{\mathrm{z},n}\int_0^t g(\zeta-(n-1)T_{\mathrm{p}})d\zeta + \bar{\Delta}_{\mathrm{z},0}\right)\right\} \quad (11)$$

for $g(t)$ a shaping filter of duration T_{p} that integrates to unity over the interval $[0,T_{\mathrm{p}}]$. The values

$$\bar{\Delta}_{\mathrm{x},0} = \frac{2\pi d}{\lambda}\sin\left(\psi_{\mathrm{C}}+\Delta_0^{\mathrm{az}}\right)\cos\left(\theta_{\mathrm{C}}+\Delta_0^{\mathrm{el}}\right) \quad (12)$$

and

$$\bar{\Delta}_{\mathrm{z},0} = \frac{2\pi d}{\lambda}\sin\left(\theta_{\mathrm{C}}+\Delta_0^{\mathrm{el}}\right) \quad (13)$$

are the initial electrical angles such that the coherent beam is initially pointed in direction $(\psi_{\mathrm{C}}+\Delta_0^{\mathrm{az}}, \theta_{\mathrm{C}}+\Delta_0^{\mathrm{el}})$.

To facilitate random spatial modulation that mimics FEM, the values of the spatial offset sequences $\{\Delta_0^{\mathrm{az}}, \Delta_1^{\mathrm{az}}, \ldots, \Delta_N^{\mathrm{az}}\}$ and $\{\Delta_0^{\mathrm{el}}, \Delta_1^{\mathrm{el}}, \ldots, \Delta_N^{\mathrm{el}}\}$ are independently drawn from a prescribed probability density function (PDF) that is formulated to subtend a solid angle in space and is symmetrical about the center look direction. For example, the center cut of a truncated Gaussian PDF is shown in Fig. 2 and is defined such that the look direction remains within ±5° of the center look direction. Figure 3 shows the same Gaussian PDF for an example look direction of $\psi_{\mathrm{C}} = 15°$ and $\theta_{\mathrm{C}} = 10°$. Note that the PDF is defined in degrees relative to the center look direction and not in terms of the absolute azimuth or elevation angle.

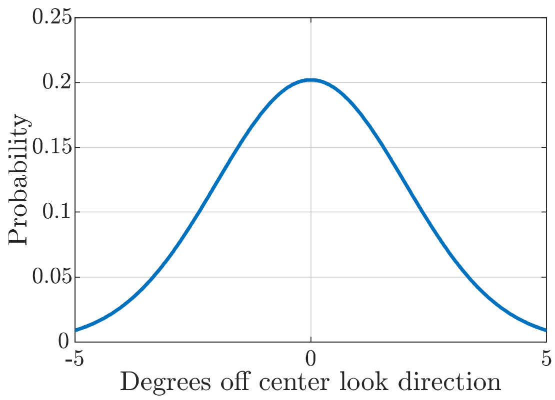

Fig. 2. Example PDF for fast-time beamsteering

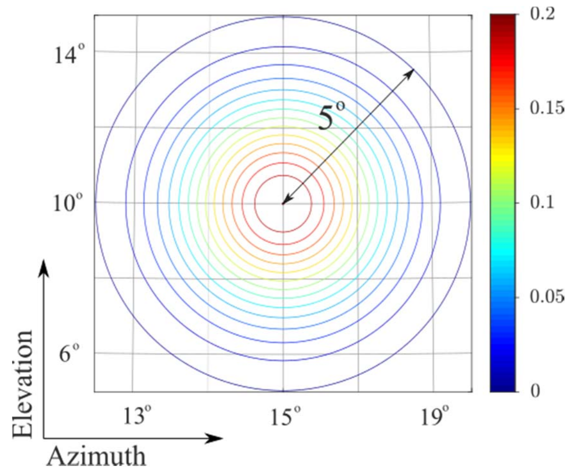

Fig. 3. 2-D PDF for center look direction $\psi_C = 15°$ and $\theta_C = 10°$

C. Combining PRO-FM with 2-D Spatial Modulation

For the ℓth PRO-FM waveform segment define a corresponding set of spatial modulation codes $\mathbf{x}_{x,\ell}$ and $\mathbf{x}_{z,\ell}$ as well as a center look direction (ψ_C, θ_C). Consequently, the center look direction can change at a rate commensurate with the time width T of a segment. When the center look direction dwells at the same location over multiple segments, it is necessary to ensure that phase discontinuities are avoided just like in (3), which is accomplished by setting the associated $\Delta_{0,\ell}^{\text{az}} = \Delta_{N,\ell-1}^{\text{az}}$ and $\Delta_{0,\ell}^{\text{el}} = \Delta_{N,\ell-1}^{\text{el}}$. Alternatively, if the center look direction transitions to a new location from segment $\ell - 1$ to segment ℓ, an additional transition stage of duration T_p is incorporated to facilitate steering of the coherent beam from the current look direction of $(\psi_{C,\ell-1} + \Delta_{N,\ell-1}^{\text{az}},\ \theta_{C,\ell-1} + \Delta_{N,\ell-1}^{\text{el}})$ to the new look direction $(\psi_{C,\ell} + \Delta_{0,\ell}^{\text{az}},\ \theta_{C,\ell} + \Delta_{0,\ell}^{\text{el}})$.

Combining the ℓth PRO-FM waveform from (3) with the spatial modulation signals from (10) and (11) therefore yields, during the ℓth segment, the set of MIMO waveforms

$$s_{\mathbf{m},\ell}(t,\psi_C,\theta_C) = \frac{1}{\sqrt{T}} s_\ell(t) \left(b_x(t;\mathbf{x}_{x,\ell})\right)^{m_x} \left(b_z(t;\mathbf{x}_{z,\ell})\right)^{m_z} \quad (14)$$

that are indexed according to array element $\mathbf{m} = (m_x, m_z)$. A normalized baseband representation of the resulting far-field emission during the ℓth segment can therefore be expressed as

$$g_\ell(t,\psi,\theta) = \frac{1}{M_x M_z} \sum_{m_x} \sum_{m_z} s_{\mathbf{m},\ell}(t)\, e^{j\left(k_x(\psi,\theta)m_x + k_z(\theta)m_z\right)} \,. \quad (15)$$

An aggregate beampattern [17-20] can likewise be defined for each segment as

$$B(\psi,\theta) = \frac{1}{TL} \sum_{\ell=1}^{L} \int_0^T \left| g_\ell(t,\psi,\theta) \right|^2 dt \,. \quad (16)$$

III. Simulation Results

To assess the efficacy of FEMR we evaluate the impact of PDF selection on the enhancement of spatial resolution and the associated trade-off in signal-to-noise ratio (SNR) loss due to beam smearing. Examples with changes in look direction and discrimination of closely-spaced scatterers are also examined.

A. Fast-time Beam-steering PDF

The PDF used to control fast-time beam steering can be of any arbitrary shape. For example, Fig. 4 again shows the truncated Gaussian, as well as a uniform distribution and what we denote as a "complementary truncated Gaussian", which is essentially the reverse of the truncated Gaussian and realizes greater diversity for spatial modulation due to the bimodal nature. Consider the response to a single scatterer for these different spatial modulation PDFs when using a $M_x = 20$ by $M_z = 20$ uniform planar array and a PRO-FM waveform with time-bandwidth product of 200. The ±5° limits on these PDFs correspond to roughly the null-to-null beamwidth for the staring case, which is ±5.7°. Note that since the array has the same number of horizontal and vertical elements, the azimuth and elevation responses are the same (so we only show azimuth).

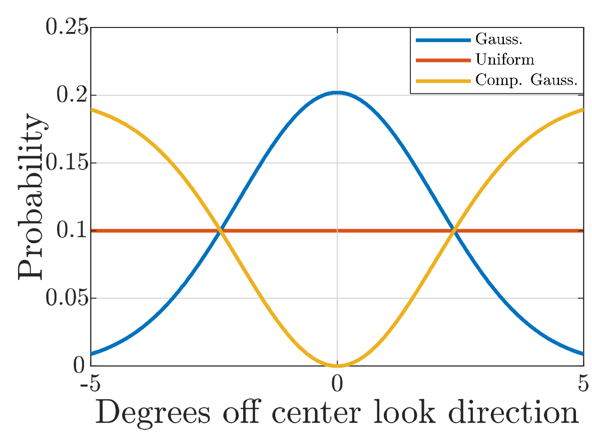

Fig. 4. Truncated Gaussian, uniform, and complementary truncated Gaussian PDFs for random spatial modulation

Along with a standard staring beam for comparison, Fig. 5 shows the top of the mainlobe for the aggregate beampattern from (16) to illustrate the SNR loss experienced when utilizing different PDFs to control the spatial modulation. When these mainlobes are normalized (Fig. 6) the enhancement in spatial resolution can also be observed. Table I lists the particular SNR loss and percent 3-dB resolution enhancement values relative to the staring beam case (100%). It is interesting to note that there appears to be a direct relationship between the amount of spatial resolution enhancement and the amount of SNR loss.

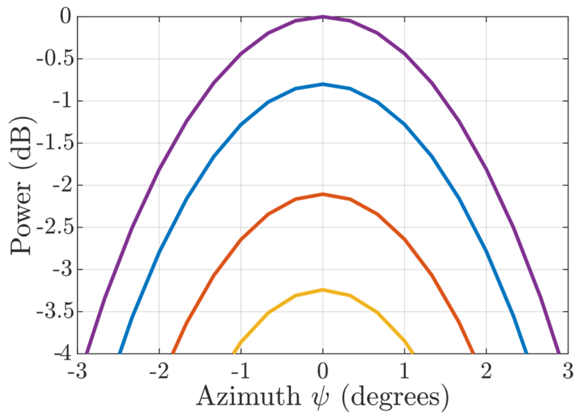

Fig. 5. Mainlobe of aggregate beampattern to show SNR loss for staring beam (purple), truncated Gaussian PDF (blue), uniform PDF (red), and complementary truncated Gaussian PDF (yellow)

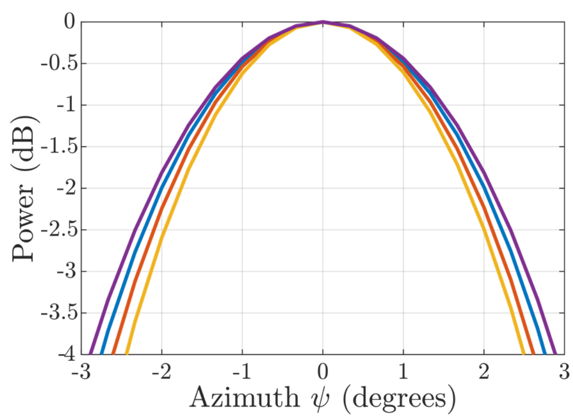

Fig. 6. Normalized mainlobe of aggregate beampattern to show resolution for staring beam (purple), truncated Gaussian PDF (blue), uniform PDF (red), and complementary truncated Gaussian PDF (yellow)

TABLE I. SPATIAL RESOLUTION ENHANCEMENT AND SNR LOSS FOR DIFFERENT RANDOM SPATIAL MODULATION PDFS

Spatial Modulation Type	*Spatial Resolution (%)*		*SNR Loss (dB)*
	Azimuth	*Elevation*	*Azimuth/Elevation*
Staring beam	100	100	0
Truncated Gaussian	95.47	95.43	0.85
Uniform	90.57	89.85	2.10
Comp. Truncated Gaussian	85.15	85.80	3.25

B. Changing Look Directions

We next consider an example in which the center look direction can change, which may be useful for tracking multiple targets. The truncated Gaussian PDF from Fig. 2 was used to control spatial modulation, with the center look direction $(\psi_{\mathrm{C}}, \theta_{\mathrm{C}})$ corresponding to the mean of the PDF. Two segments of individual time-bandwidth product of 200 were generated using PRO-FM. Each segment was over-sampled by a factor of 4 relative to 3-dB bandwidth to provide sufficient fidelity.

These waveform segments were emitted in respective center look directions of (0°, −25°) and (15°, 10°) using independent random spatial modulation codes. Figure 7 depicts the aggregate beampattern in wavenumber space where two clear mainlobes are evident. To provide a more time-dependent view of the coherent beam movement, Fig. 8 shows a trace of the instantaneous peak of the coherent beam, where the random nature imposed upon the beam steering can be easily observed.

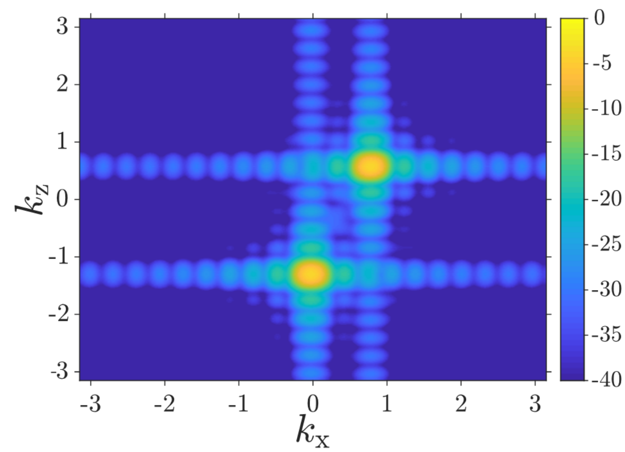

Fig. 7. Aggregate beam pattern in wavenumber space for the random spatial modulation illuminating of two different look directions

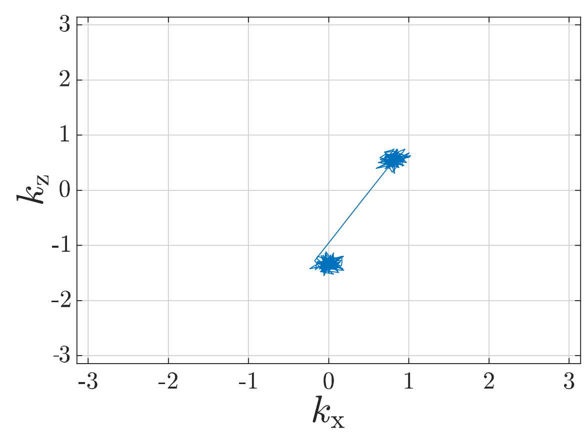

Fig. 8. Trace of the instantaneous peak of the coherent beam for fast-time random spatial modulation illuminating two distinct look directions

C. Discrimination of Closely-spaced Scatterers

Finally, consider the illumination of a scene containing the arrangement of scatterers depicted in Fig. 9 and illuminated with three different emission structures, all using the same underlying PRO-FM waveform. Each scatterer was scaled to produce a receive SNR of 20 dB if illuminated directly with a staring beam and had independent random phase. Figure 10 depicts cuts of the response when applying matched filtering according to the far-field emission for a staring beam, where the matched filter in this case is the same for all spatial directions. In Fig. 10 the four scatterers in the azimuth/elevation cut are not discernibly separable and neither are the center two scatterers in the range/elevation cut.

In Fig. 11, phase-only beam spoiling [32] is employed through a modest random (yet static) dithering of the staring beam on transmit, the purpose of which is to provide a slightly wider illumination coverage of the target scene. Compared to the staring beam from Fig. 10, the dithered beam does appear to provide a bit more visibility for the scatterers in the azimuth/elevation cut, though there is only modest improvement in the range/elevation cut.

Lastly, Fig. 12 shows how random spatial modulation can more clearly identify the four scatterers in the azimuth/elevation cut. Due to the enhanced spatial separability of this emission scheme the scatterers in the range/elevation cut are also now clearly identifiable.

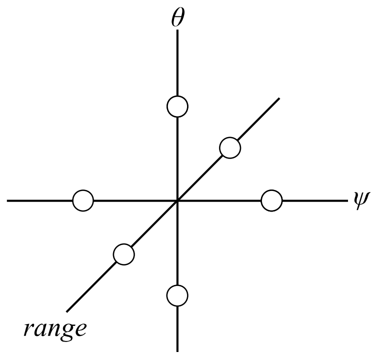

Fig. 9. Arrangement of scatterers in range, azimuth, and elevation, where the spatial separation is ±4.5° relative to the center look direction at the origin

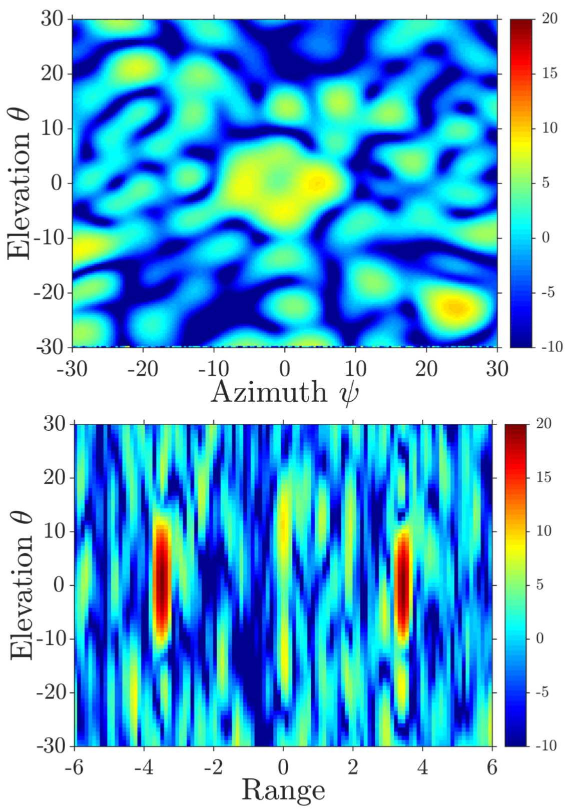

Fig. 10. Azimuth-elevation cut (top) and range-elevation cut (bottom) for a staring beam with null-to-null beamwidth of ±5.7°

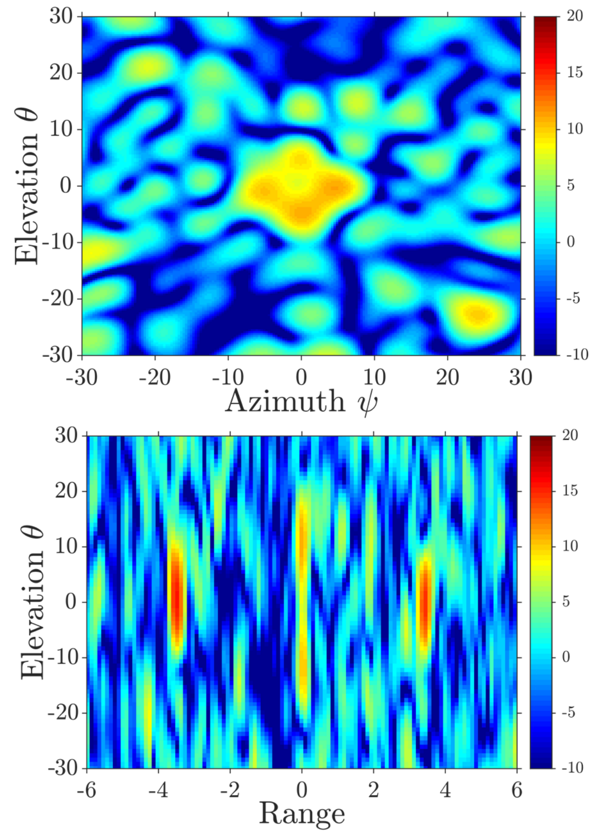

Fig. 11. Azimuth-elevation cut (top) and range-elevation cut (bottom) for a static spatially-dithered beam

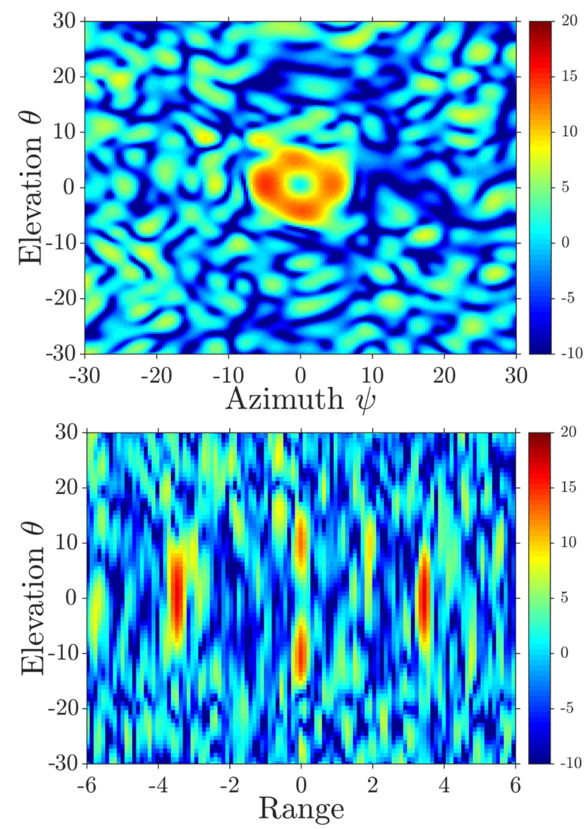

Fig. 12. Azimuth-elevation cut (top) and range-elevation cut (bottom) for a spatially-modulated beam using a complementary truncated Gaussian PDF

IV. CONCLUSIONS

A randomized generalization to the notion of spatial modulation denoted as fixational eye movement radar (FEMR) has been presented and evaluated. This formulation mimics the actuation of the human eye via an active MIMO radar emission in which the coherent beam moves in fast-time in random directions around the vicinity of a center look direction. It has been demonstrated in simulation that, compared to a standard staring beam and a static dithered beam, the fast-time random movement of FEMR facilities enhanced discrimination of scatterers that are closely spaced in azimuth and elevation. Further, there are myriad different spatial modulation PDFs one could choose, though there does appear to be a linkage between the amount of resolution improvement and SNR loss. It was shown in [33] that the space/fast-time coupling inherent to spatially modulated emissions likewise enhances structured adaptive receive processing.

REFERENCES

[1] M. Vespe, G. Jones, C.J. Baker, "Lesson for radar: waveform diversity in echolocating mammals," *IEEE Signal Processing Mag.*, vol. 26, no. 1, pp. 65-75, Jan. 2009.

[2] T.G. Leighton, S.D. Meers, P.R. White, "Propagation through nonlinear time-dependent bubble clouds and the estimation of bubble populations from measured acoustic characteristics," *Proc. Royal Society of London A*, vol. 460, pp. 2521–2550, Sept. 2004.

[3] C.J. Baker, G.E. Smith, A. Balleri, M. Holderied, H.D. Griffiths, "Biomimetic echolocation with application to radar and sonar sensing," *Proc. IEEE*, vol. 102, no. 4, pp. 447-458, Apr. 2014.

[4] H.U. Schnitzler, E.K.V. Kalko, "Echolocation by insect-eating bats," *Bioscience*, vol. 51, pp. 557-569, 2001.

[5] K. Ghose, C.F. Moss, "Sonar beam pattern of a flying bat as it tracks tethered insects," *J. Acoust. Soc. Am.*, vol. 114, no. 2, pp. 1120-1131, Aug. 2003.

[6] J.R. Potter, E.A. Taylor, "On novel reception models for bottlenose dolphin echolocation," *Proc. Inst. Acoustics*, vol. 24, 2002.

[7] T.G. Leighton, G.H. Chua, P.R. White, "Do dolphins benefit from nonlinear mathematics when processing their sonar returns?," *Proc. Royal Society A*, vol. 468, pp. 3517-3532, 2012.

[8] G.H. Chua, P.R. White, T.G. Leighton, "Use of clicks resembling those of the Atlantic bottlenose dolphin (*Tursiops truncatus*) to improve target discrimination in bubbly water with biased pulse summation sonar," *IET Radar, Sonar and Navigation*, vol. 6, no. 6, pp. 510–515, July 2012.

[9] W.W.L. Au, S.W. Martin, "Why dolphin biosonar performs so well in spite of mediocre 'equipment'," *IET Radar, Sonar & Navigation*, vol. 6, no. 6, pp. 566-575, July 2012.

[10] T.G. Leighton, S.D. Richards, P.R. White "Marine mammal signals in bubbly water," *Proc. Inst. Acoustics*, 2004.

[11] M. Wicks, E. Mokole, S.D. Blunt, V. Amuso, R. Schneible, eds., *Principles of Waveform Diversity and Design*, SciTech Publishing, 2010.

[12] S.D. Blunt, E.L. Mokole, "An overview of radar waveform diversity," *IEEE AESS Systems Magazine*, vol. 31, no. 11, pp. 2-42, Nov. 2016,

[13] M. Rolfs, "Microsaccades: small steps on a long way," *Vision Research*, vol. 49, pp. 2415-2441, 2009.

[14] E. Ahissar, A. Arieli, "Seeing via miniature eye movements: a dynamic hypothesis for vision," *Frontiers in Computational Neuroscience*, vol. 6, no. 89, Nov. 2012.

[15] J. Cui, M. Wilke, N.K. Logothetis, D.A. Leopold, H. Liang, "Visibility states modulate microsaccade rate and direction," *Vision Research*, vol. 49, pp. 228-236, 2009.

[16] S. Haykin, Y. Xue, P. Setoodeh, "Cognitive radar: step toward bridging the gap between neuroscience and engineering," *Proc. IEEE*, vol. 100, no. 11, pp. 3102-3130, Nov. 2012.

[17] S.D. Blunt, P. McCormick, T. Higgins, M. Rangaswamy, "Spatially-modulated radar waveforms inspired by fixational eye movement," *IEEE Radar Conf.,* Cincinnati, OH, May 2014.

[18] S.D. Blunt, P. McCormick, T. Higgins, M. Rangaswamy, "Physical emission of spatially-modulated radar," *IET Radar, Sonar, and Navigation,* vol. 8, no. 12, pp. 1234-1246, Dec. 2014.

[19] P. McCormick, S.D. Blunt, "Fast-time 2-D spatial modulation of physical radar emissions," *Intl. Radar Symposium*, Dresden, Germany, June 2015.

[20] J. Jakabosky, P. McCormick, S.D. Blunt, "Implementation & design of physical radar waveform diversity," *IEEE AESS Systems Mag.*, vol. 31, no. 12, pp. 26-33, Dec. 2016.

[21] S.D. Blunt, M. Cook, J. Jakabosky, J. de Graaf, E. Perrins, "Polyphase-coded FM (PCFM) radar waveforms, part I: implementation," *IEEE Trans. Aerospace & Electronic Systems,* vol. 50, no. 3, pp. 2218-2229, July 2014.

[22] P. Antonik, M.C. Wicks, H.D. Griffiths, C.J. Baker, "Frequency diverse array radars," *IEEE Radar Conf.*, Verona, NY, Apr. 2006.

[23] T. Higgins, S. Blunt, "Analysis of range-angle coupled beamforming with frequency-diverse chirps," *Intl. Waveform Diversity & Design Conf.*, Orlando, FL, Feb. 2009.

[24] P.F. Sammartino, C.J. Baker, H.D. Griffiths, "Frequency diverse MIMO techniques for radar," *IEEE Trans. Aerospace & Electronic Systems*, vol. 49, no. 1, pp. 201-222, Jan. 2013.

[25] W.-Q. Wang, H.C. So, A. Farina, "An overview on time/frequency modulated array processing," *IEEE J. Selected Topics Signal Processing*, vol. 11, no. 2, pp. 228-246, Mar. 2017.

[26] J. Jakabosky, S. D. Blunt, B. Himed, "Waveform design and receive processing for nonrecurrent nonlinear FMCW radar," *IEEE Intl. Radar Conf.*, Arlington, VA, May 2015.

[27] J. Jakabosky, S. D. Blunt, B. Himed, "Spectral-shape optimized FM noise radar for pulse agility," *IEEE Radar Conf.*, Philadelphia, PA, May 2016.

[28] C.A. Mohr, P.M. McCormick, S.D. Blunt, and C. Mott, "Spectrally-efficient FM noise radar waveforms optimized in the logarithmic domain," *IEEE Radar Conf.*, Oklahoma City, OK, Apr. 2018.

[29] A. Levi, H. Stark, "Image restoration by the method of generalized projections with application to restoration from magnitude," *IEEE Intl. Conf. Acoustics, Speech, & Signal Processing*, Mar. 1984.

[30] H.H. Bauschke, P.L. Combettes, D.R. Luke, "Phase retrieval, error reduction algorithm, and Fienup variants: a view from convex optimization," *J. Optical Soc. Am. A*, vol. 19, no. 7, pp. 1334–1345, July 2002.

[31] Van Trees, H. L., *Optimum Array Processing*, John Wiley & Sons, 2002.

[32] J.C. Kerce, G.C. Brown, M.A. Mitchell, "Phase-only transmit beam broadening for improved radar search performance," *IEEE Radar Conf.*, Waltham, MA, Apr. 2007.

[33] P. McCormick, T. Higgins, S.D. Blunt, M. Rangaswamy, "Adaptive receive processing of spatially-modulated physical radar emissions," *IEEE J. Selected Topics Signal Processing*, vol. 9, no. 8, pp. 1415-1426, Dec. 2017.